

Expected insights on type Ia supernovae from LISA's gravitational wave observations

Valeriya Korol¹, Riccardo Buscicchio^{2,3}, Ruediger Pakmor¹, Javier Morán-Fraile⁴, Christopher J. Moore^{5,6,7}, and Selma E. de Mink¹

¹ Max-Planck-Institut für Astrophysik, Karl-Schwarzschild-Straße 1, 85748 Garching, Germany
e-mail: korol@mpa-garching.mpg.de

² Dipartimento di Fisica “G. Occhialini”, Università degli Studi di Milano-Bicocca, Piazza della Scienza 3, 20126 Milano, Italy

³ INFN, Sezione di Milano-Bicocca, Piazza della Scienza 3, 20126 Milano, Italy

⁴ Heidelberger Institut für Theoretische Studien (HITS), Schloss-Wolfsbrunnengasse 35, 69118 Heidelberg, Germany

⁵ Institute of Astronomy, University of Cambridge, Madingley Road, Cambridge, CB3 0HA, UK

⁶ Kavli Institute for Cosmology, University of Cambridge, Madingley Road, Cambridge, CB3 0HA, UK

⁷ Department of Applied Mathematics and Theoretical Physics, Centre for Mathematical Sciences, University of Cambridge, Wilberforce Road, CB3 0WA, UK

Received July 4, 2024

ABSTRACT

The nature of progenitors of type Ia supernovae have long been debated, primarily due to the elusiveness of the progenitor systems to traditional electromagnetic observation methods. We argue that gravitational wave observations with the upcoming Laser Interferometer Space Antenna (LISA) offer the most promising way to test one of the leading progenitor scenarios — the double-degenerate scenario, which involves a binary system of two white dwarf stars. In this study, we review published results, supplementing them with additional calculations for the context of type Ia supernovae. We discuss that LISA will be able to provide a complete sample of double white dwarf type Ia supernova progenitors with orbital period less than 16–11 minutes (gravitational wave frequencies above 2–3 milli-Hertz). Such a sample will enable a statistical validation of the double-degenerate scenario by simply counting whether LISA detects enough double white dwarf binaries to account the measured type Ia merger rate in Milky Way-like galaxies. Additionally, we illustrate how LISA's capability to measure the chirp mass will set lower bounds on the primary mass, revealing whether detected double white dwarf binaries will eventually result in a type Ia supernova. We estimate that the expected LISA constraints on the type Ia merger rate for the Milky Way will be 4–9%. We also discuss the potential gravitational wave signal from a type Ia supernova assuming a double detonation mechanism and explore how multi-messenger observations could significantly advance our understanding of these transient phenomena.

Key words. Gravitational waves – binaries (including multiple): close – white dwarfs – supernovae: type Ia

1. Introduction

Type Ia supernovae (SNe Ia) are amongst the most energetic explosions in the Universe, producing a luminosity of about 10^{43} erg s⁻¹ near maximum light. They emerged as a distinct class based on spectral signatures: the absence of hydrogen and helium, with broad features of silicon, calcium and iron (e.g., see a review by Filippenko 1997). Notably, light curves shapes of many SNe Ia closely resemble each other: peaking within 15–20 days and then declining rapidly. As a consequence, these standardisable (also refereed to as ‘normal’) SNe Ia have been adopted as cosmological standard candles and provided the first evidence for the acceleration of cosmic expansion (Riess et al. 1998; Perlmutter et al. 1999). The luminosity that characterises the light curve of a (normal) SN Ia originates from the radioactive decay of ⁵⁶Ni to ⁵⁶Co and then to stable ⁵⁶Fe. The energetics and chemical composition implies that this class of SNe result from the thermonuclear combustion of a white dwarf (Hoyle & Fowler 1960). Despite SNe Ia being among the most studied transient phenomena, there is still no consensus on other fundamental aspects such as the nature of the progenitor and explosion mechanisms, both from theoretical and observational perspec-

tives (see recent reviews by Maoz et al. 2014; Ruitter 2020; Liu et al. 2023).

There is a broad consensus that the white dwarf explosion in a SN Ia is triggered by the interaction with a companion star. Identifying the nature of the companion (and the nature of the explosion) however, has been a long-standing challenge (e.g., Livio & Mazzali 2018). Historically, the field has developed around two main progenitor scenarios: single-degenerate and double-degenerate¹. In the single-degenerate scenario, a white dwarf accretes matter from a non-degenerate companion (e.g., a main sequence star, sub-giant, or helium star) until it approaches the Chandrasekhar mass limit and explodes (Whelan & Iben 1973; Nomoto et al. 1984). In contrast, in the double-degenerate scenario, the companion is another white dwarf, and the two white dwarfs are brought together to interact (or directly to merge) by gravitational wave (GW) radiation (Whelan & Iben 1973; Iben & Tutukov 1984). Each scenario offers a plausible explanation, yet in the absence of definitive evidence, it remains impossible to conclusively favour one over the other (e.g., Maoz et al. 2014).

¹ Here ‘degenerate’ refers to white dwarfs, which are supported by the pressure of degenerate electrons, in contrast to normal (non-degenerate) stars, which are supported by thermal pressure.

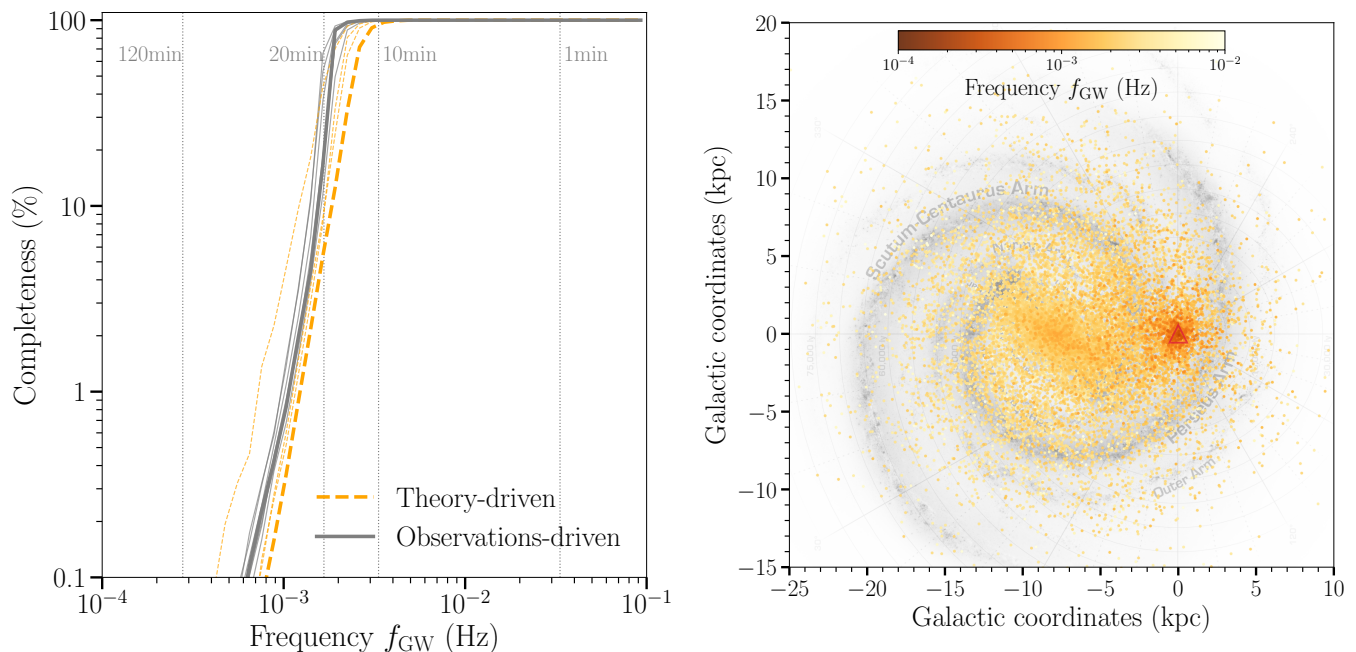


Fig. 1. Left panel: The completeness of LISA’s Galactic WD+WD sample as a function of frequency is estimated based on sets of mock Galactic catalogues: theory-driven (dashed orange lines, Korol et al. 2017; Wilhelm et al. 2021) and observations-driven (solid grey lines, Korol et al. 2022). Thick lines represent the respective default models, while thin lines represent model variations within each set (e.g., different prescriptions for binary interactions in the theory-driven models). Vertical dotted lines mark the respective binary orbital periods. **Right panel:** The spatial distribution of binaries with $\rho_{1\text{yr}} \geq 7$ within the Galaxy adapted from Wilhelm et al. (2021), colour-coded by GW frequency. In the background the artist impression of our current view of the Milky Way. The red triangle at (0, 0) shows LISA’s position, while the Galactic Centre is at $(-8.2, 0)$.

Here we explore the SNe Ia progenitor question from the perspective of future GW observations. Specifically, we discuss the potential of the upcoming *Laser Interferometer Space Antenna* (LISA), a milli-Hertz GW observatory that has been recently adopted and scheduled for launch by the European Space Agency in mid 2030s (Colpi et al. 2024). Our arguments still hold for other space-based milli-Hertz GW observatories like *TianQin* (Luo et al. 2016; Huang et al. 2020) and *Taiji* (Ruan et al. 2018). LISA’s sensitivity to the shortest period (less than about 2 hours) double white dwarf (WD+WD) binaries in the Milky Way and its nearest satellite galaxies presents a unique opportunity to test the double-degenerate scenario directly (Amaro-Seoane et al. 2023). Rebassa-Mansergas et al. (2019) highlighted the significant challenges associated with detecting double-degenerate SN Ia progenitors through electromagnetic (EM) observations, primarily due to the intrinsic faintness of these binaries. Even with next-generation large-aperture telescopes, such as the European Extremely Large Telescope (E-ELT), the estimated probability of identifying and validating (by measuring the binary components’ masses) SN Ia progenitors is remarkably low. Here we show why GW observations with LISA offer a promising alternative for determining the nature of SN Ia progenitor systems, overcoming the limitations faced by traditional EM observation methods.

The structure of this work is as follows. In Section 2, we review the constraints on double-degenerate WD+WD progenitors in the Milky Way expected based on the LISA observations, including the number of these binaries (Section 2.1), chirp mass constraints (Section 2.2), and their overall merger rate (Section 2.3). These constraints will likely be delivered by LISA (Colpi et al. 2024). In Section 3, we discuss the fortunate possibility of directly observing of the final inspiral and the SN Ia event while LISA is operational. We adopt a 3D hydro-

dynamical simulation, in which the primary white dwarf undergoes the double detonation mechanism, to illustrate the evolution of GW strain in frequency over the last few orbits leading to the SN Ia event (Section 3.1). We also discuss implications of multi-messenger observations (Section 3.2). Finally, we present the summary and conclusions in Section 4.

2. Constraints on the double-degenerate progenitor systems in the Milky Way

The dense and compact nature of white dwarf stars, while challenging for EM observations, offers advantages for the GW detection. In fact, in the following we argue that the best way of surveying double-degenerate SN Ia progenitors is via GW observations with a mission like LISA.

GW radiation from a circular WD+WD can be modelled with a nearly monochromatic sinusoidal waveform (e.g., LISA Consortium Waveform Working Group et al. 2023). Such a waveform can be described by eight key parameters: the GW amplitude \mathcal{A} , GW frequency f_{GW} , its derivative \dot{f}_{GW} , binary’s sky coordinates (λ, β) , inclination angle ι , polarisation angle ψ , and the initial phase ϕ_0 . For circular binaries, the GW frequency is exactly $f_{\text{GW}} = 2/P_{\text{orb}}$ with P_{orb} being the binary’s orbital period. The strain amplitude of the signal is given by

$$\mathcal{A} = \frac{2(G\mathcal{M})^{5/3}}{c^4 d} (\pi f_{\text{GW}})^{2/3}, \quad (1)$$

and is determined by the binary’s GW frequency, distance d and chirp mass $\mathcal{M} = (m_1 m_2)^{3/5} / (m_1 + m_2)^{1/5}$, for component masses $m_1 \geq m_2$; G and c are respectively the gravitational constant and speed of light. Equation 1 reveals that binaries characterised by higher frequencies and larger masses produce GWs with larger

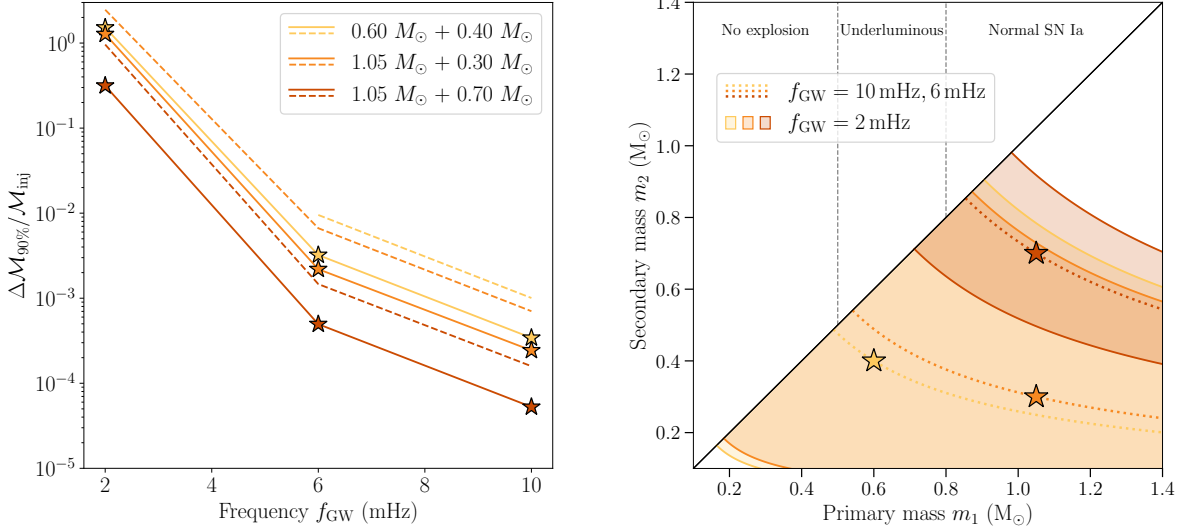


Fig. 2. LISA’s capability to measure chirp masses and to constrain the binary component masses. **Left panel:** Fractional uncertainty on the chirp mass, with solid (dashed) lines representing face-on (edge-on) binary configurations. Stars denote representative simulated systems. **Right panel:** Constraints on component masses, with shaded areas between solid lines denoting sources at 2 mHz. Dotted lines represent sources at 6 and 10 mHz. These constraints assume that the symmetric mass ratio (i.e. $m_1 m_2 / (m_1 + m_2)^2$) is unknown and are sampled from a uniform prior. Vertical dashed grey lines delimit three representative classes: configurations producing no explosion ($m_1 < 0.5 M_{\odot}$), those likely resulting in a low-luminosity thermonuclear transient ($0.5 < m_1 < 0.8 M_{\odot}$), and those that will likely result in a normal SN Ia ($m_1 > 0.8 M_{\odot}$).

amplitude, yielding signals with higher signal-to-noise ratio:

$$\rho \propto \mathcal{A} \sqrt{\frac{T_{\text{obs}}}{S_n(f_{\text{GW}})}}, \quad (2)$$

where T_{obs} is the observation time and $S_n(f_{\text{GW}})$ is the noise power spectral density, quantity describing the noise of the LISA detector as a function of frequency (e.g., Moore et al. 2015), at the binary’s frequency (for the full derivation see Finch et al. 2023, Appendix A). We note that, unlike EM observations — which are based on the measurement of energy flux and scale with $1/d^2$ — GW observations offer direct measurements of the signal’s amplitude and thus scale with $1/d$. Consequently, GW observations enable the detection of EM-dim sources – or even entirely invisible dormant binary black holes – at distances that are not (directly) accessible with EM observations (e.g., Sesana et al. 2020).

2.1. Probing the number of progenitor system

To study the expected completeness of LISA’s WD+WD sample, we utilise published mock catalogues assembled based on both theory-driven (Korol et al. 2017; Wilhelm et al. 2021) and observations-driven (Korol et al. 2022) population synthesis. Our theory-driven models are based on the SEBA stellar and binary evolution module (Portegies Zwart & Verbunt 1996; Nelemans et al. 2001; Toonen et al. 2012) with variations in the underlying assumptions for the binary interactions (for details see Toonen et al. 2012). While our observations-driven models are based on a statistical method developed to characterise the binarity of large spectroscopic samples of white dwarfs with sparsely sampled radial velocity data (Maoz et al. 2012; Badenes & Maoz 2012; Maoz et al. 2018). Variations in our observations-driven models are due different underlying assumptions for the binary fraction, WD+WD separation (at formation) and mass distributions (for details see Korol et al. 2022).

We assess the completeness as the percentage of detectable binaries relative to the total underlying WD+WD population as a function of frequency. Importantly, the populations selected for this study are directly comparable, as they were analysed under the same mission specifications, including the noise model, a 4-year mission duration, and a detection threshold of $\rho_{4\text{yr}} = 7$. This analysis employed the same pipeline as Karnesis et al. (2021), which self-consistently estimates the unresolved stochastic foreground from the input population and resolves binaries with a signal-to-noise ratio above the threshold. The result is presented in the left panel of Fig. 1, where solid grey lines represent the family of observations-driven models and orange dashed lines represent the family of theory-driven models. In the right panel, we show the example of the spatial distribution within the Milky Way of WD+WD binaries with $\rho_{1\text{yr}} \geq 7$ from Wilhelm et al. 2021, colour-coded by GW frequency. It is evident that binaries emitting at $f_{\text{GW}} \geq 2 - 3$ mHz (in the pale-orange to yellow) can be detected throughout the entire Galaxy. Although not strictly comparable due to differences in the WD+WD detection analysis, we expect that other recently published models will show similar results (e.g., Lamberts et al. 2019; Breivik et al. 2020; Li et al. 2020; Thiele et al. 2023; Tang et al. 2024).

Figure 1 illustrates that, LISA is expected to achieve a complete sample of WD+WD binaries with GW frequencies above 2–3 mHz, corresponding to orbital periods shorter than 16 to 11 minutes. Thus, based on the LISA sample, we would be able to quantitatively assess the contribution of double-degenerate progenitors to the measured SN Ia merger rate in from EM observations (see also Colpi et al. 2024). This could be achieved by simply counting whether LISA detects enough WD+WD binaries, importantly without concerns regarding selection effect.

2.2. Probing the masses of progenitor system

To identify potential SN Ia progenitors within LISA’s sample, constraints on the binary components’ masses are essential, particularly considering that only a subset of the most massive WD+WD binaries (with primary mass $m_1 > 0.8 M_\odot$) are more likely to lead to SN Ia events. This is an essential requirement because lower mass white dwarfs may not produce significant amounts of ^{56}Ni , even if they undergo a thermonuclear explosion (e.g., Sim et al. 2010). We also assume that binaries $0.5 < m_1 < 0.8 M_\odot$ result in thermonuclear explosions of lower luminosity than a ‘normal’ SN Ia, while those with $m_1 < 0.5 M_\odot$ fail to detonate (e.g., Morán-Fraile et al. 2024; Shen et al. 2024).

At GW frequencies greater than 2-3 mHz, LISA is expected to measure not only the GW frequency and amplitude of WD+WD signals but also the frequency derivative – the so-called *chirp* – resulting from GW radiation (e.g., Colpi et al. 2024). Through the measurement of f_{GW} and its derivative \dot{f}_{GW} , it becomes possible to deduce the binary system’s chirp mass. Under the assumptions that the binary is detached, non-interacting, and on a circular orbit, which are expected to hold for most of the LISA-detectable WD+WD population, the GW frequency derivative can be expressed as:

$$\dot{f}_{\text{GW}} = \frac{96 (GM)^{5/3}}{5 \pi c^5} (\pi f_{\text{GW}})^{11/3}. \quad (3)$$

We note that the above expression ignores tidal effects, which could become important at higher frequencies for example binaries considered below (e.g., Shah & Nelemans 2014; Wolz et al. 2021; Toubiana et al. 2024). We also note that ignoring these effects, especially at $f_{\text{GW}} > 10$ mHz, can lead to non-negligible biases in the mass estimate (Fiacco et al. 2024).

To showcase LISA’s potential for measuring the chirp mass of double-degenerate SN Ia progenitor systems, we consider three examples: $0.6 M_\odot + 0.4 M_\odot$, $1.05 M_\odot + 0.3 M_\odot$, and $1.05 M_\odot + 0.7 M_\odot$. These combinations yield chirp masses of $0.42 M_\odot$, $0.47 M_\odot$, and $0.74 M_\odot$, respectively. The binary with the lowest chirp mass is representative of a potential progenitor for thermonuclear transients of lower luminosity than a ‘normal’ SN Ia, whereas the latter two configurations are representative of a ‘normal’ SN Ia progenitor (e.g., Shen 2015). We generate GW signals and perform parameter estimation for these three example binaries within a Bayesian inference framework using Balrog (Buscicchio et al. 2019; Roebber et al. 2020; Buscicchio et al. 2021; Klein et al. 2022; Finch et al. 2023). We simulate signals with initial frequencies of 2, 6 and 10 mHz, while bracketing dependence on binaries’ orientation with face-on and edge-on configurations. All sources are (arbitrarily) located in the Galactic centre, assuming distance of 8.2 kpc (e.g., GRAVITY Collaboration et al. 2021).

In Fig. 2 we showcase LISA’s expected capability to measure the binary’s chirp mass across different frequencies (left panel) and the corresponding constraints on the component masses (right panel). Our results reveal that at 2 mHz, the chirp mass measurements is constraining only for the most massive case among the considered examples. As the frequency increases beyond 4-5 mHz, the precision of the chirp mass measurements significantly improves for all three examples, dropping rapidly to 0.01% - 0.001% at 10 mHz. From the right panel, we observe that at 2 mHz (as indicated by coloured bands), the chirp mass measurement implies a minimum primary mass of $0.2 M_\odot$ for the binaries with chirp masses of $0.42 M_\odot$ and the $0.47 M_\odot$, and a minimum mass of $0.7 M_\odot$ for the one with a $0.74 M_\odot$ chirp mass. Consequently, for the latter example, we can predict an eventual

SN Ia with a posterior probability of 96%, estimated by assuming a uniform prior in mass ratio and by counting posterior samples within the $m_1 > 0.8 M_\odot$ region. As the frequency increases to 6 mHz and higher, the uncertainty in chirp mass measurement reduces to less than 1%; as a consequence, constraints on components’ mass converge to a line. This precision translates to a lower bound for the primary mass of $0.49 M_\odot$ for the $0.42 M_\odot$ chirp mass binary, and $0.55 M_\odot$ for the $0.47 M_\odot$ chirp mass binary. For these two cases, the probability of eventually resulting in a thermonuclear transient is 100%, estimated by assuming a uniform prior in mass ratio and by counting posterior samples within the $m_1 > 0.5 M_\odot$ region. For the most massive of the considered examples, the lower limit on the primary mass can be set to $0.87 M_\odot$. This implies that LISA will be able to assign a 100% probability for this binary to be a progenitor of a ‘normal’ SN Ia (i.e., $m_1 > 0.8 M_\odot$).

2.3. Probing the merger rate of progenitor systems

The measurement of the chirp mass offers a method to estimate the time until merger due to GW radiation. The time to merger, $\tau = t_{\text{merger}} - t$, can be estimated, in a first post-Newtonian approximation, by integrating Eq. 3 (e.g., Peters 1964)

$$\tau(f_{\text{GW}}, \mathcal{M}) = \frac{5c^5}{256(GM)^{5/3}(\pi f_{\text{GW}})^{8/3}}, \quad (4)$$

which is valid under the same assumptions as used in Eq. 3. Given that the GW frequency of WD+WD binaries is measured with high precision ($\Delta f_{\text{GW}}/f_{\text{GW}} \ll 10^{-5}$, e.g., Karnesis et al. 2021; Finch et al. 2023; Colpi et al. 2024), the uncertainty in τ primarily depends on LISA’s ability to constrain the chirp mass, with $\Delta\tau/\tau \approx 5/3 \Delta\mathcal{M}/\mathcal{M}$. We provide the estimate of this measurement for the three considered examples in Table 1.

Assuming that binaries in the LISA sample inspiral according to Eq. 4, their distribution in frequency will enable the estimate of the overall merger rate. To provide an order-of-magnitude estimate of LISA’s ability to constrain the SNe Ia merger rate, $\mathcal{R}_{\text{SNIa}}$, let us consider a simplified scenario where all SNe Ia progenitors consist of binaries with masses of $1.05 M_\odot + 0.7 M_\odot$ (corresponding chirp mass of $0.74 M_\odot$). As illustrated in Section 2.2, binaries with similar chirp mass or higher can be identified as SN Ia progenitors with high confidence, starting at 2 mHz. Assuming that the WD+WD population is in a steady state, the spectral density of binaries resolved over the mission duration is given by

$$\frac{dN_{\text{SNIa}}}{df_{\text{GW}}} = \frac{5c^5 \mathcal{R}_{\text{SNIa}}}{96\pi^{8/3} (GM)^{5/3} f_{\text{GW}}^{11/3}}. \quad (5)$$

The rate can be recovered by integrating the above equation over frequency and solving for $\mathcal{R}_{\text{SNIa}}$:

$$\mathcal{R}_{\text{SNIa}} = \frac{256(GM)^{5/3} (\pi f_{\text{GW}})^{8/3}}{5c^5} N_{\text{SNIa}}(> f_{\text{GW}}), \quad (6)$$

where $N_{\text{SNIa}}(> f_{\text{GW}})$ is the total number of binaries emitting above a certain frequency threshold f_{GW} . From Eq. 6 it follows that the error on $\mathcal{R}_{\text{SNIa}}$ depends on the errors in the number count of SN Ia progenitor binaries and the error on the chirp mass. As discussed in Section 2.1, at frequencies higher than 2 mHz, LISA can detect every relevant binary, allowing the estimate of the merger rate of $1.05 M_\odot + 0.7 M_\odot$ without concerns about selection effects.

To estimate the error on $\mathcal{R}_{\text{SNIa}}$, we first sample $N_{\text{SNIa}}(> f_{\text{GW}})$ from a Poisson distribution with the mean set by assuming SN Ia merger rates of $(2, 4, 7) \times 10^{-3} \text{ yr}^{-1}$ (e.g., Cappellaro & Turatto 2001; Li et al. 2011; Maoz et al. 2018), derived based on EM observations. Our assumption on the underlying ‘true’ merger rate sets the number of detected binaries, which we then distribute in frequency according to Eq. 5. As a reference, setting SN Ia merger rate to $2 \times 10^{-3} \text{ yr}^{-1}$ ($7 \times 10^{-3} \text{ yr}^{-1}$) yields 1069, 57, 15 (3743, 200, 51) binaries with a chirp mass of $0.74 M_{\odot}$ at frequencies above 2, 6, and 10 mHz, respectively. To mimic the effects of measurement uncertainties, each chirp mass measurement is subsequently drawn from a Gaussian distribution, the width of which is interpolated from our results for the posterior widths for the $1.05 M_{\odot} + 0.7 M_{\odot}$ binary in Fig. 2. We perform Monte Carlo simulations over an arbitrarily large number of realisations. The result is illustrated in Fig. 3 (solid lines); for comparison, we also plot the number count error only (dashed lines). This experiment demonstrates that LISA’s error on the merger rate including binaries at $f_{\text{GW}} < 4 \text{ mHz}$ will be dominated by the large number of binaries with relatively poor constraints on the chirp mass ($\sim 10\%$, cf. Fig. 2). These binaries are about an order of magnitude more numerous than those at $f_{\text{GW}} > 4 \text{ mHz}$, where the chirp mass constraint improves to $\sim 1\%$ level and better. On the other hand, in the sample including binaries with $f_{\text{GW}} > 4 \text{ mHz}$, the error is primarily driven by the Poissonian error given the lower number of sources ($< 50 - 10$ at $f_{\text{GW}} > 10 \text{ mHz}$ for the considered SN Ia rates). The measurement is optimal for the sub-sample of binaries with frequencies less than 4 mHz, where, based on the LISA observations alone, we achieve SN Ia merger rate error below 10%. It might also be possible to obtain an improved measurement of the rate $\mathcal{R}_{\text{SNIa}}$ (i.e. with a smaller uncertainty) by also using the larger, but incomplete, sample of binaries with lower frequencies, although this would require a more detailed population-level, hierarchical analysis that accounts for selection effects.

If the merger rate of WD+WD LISA sources inferred in this way turns out to be consistent with the known rate of SNe Ia, this would be persuasive evidence in favour of the double-degenerate scenario. If, on the other hand, the rates do not match then this suggests that a least some fraction of SNe Ia come from another channel.

3. The chance of a direct observation of the final inspiral and SN Ia

As discussed in Section 2, the double-degenerate SN Ia progenitor scenario can already be confirmed or rejected based on the number/merger rate of close, massive WD+WD binaries that LISA will detect across our Galaxy. Given the observed SN Ia rate in the Milky Way-like galaxies, $\mathcal{R}_{\text{SNIa}} = (3 - 7) \times 10^{-3} \text{ yr}^{-1}$ (e.g., Cappellaro & Turatto 2001; Li et al. 2011; Maoz et al. 2018), we expect a 3 – 7% chance of a SN Ia event during LISA’s maximum lifetime of 10 yr. Additionally, the most massive SN Ia WD+WD progenitors LISA can observe in the Magellanic Clouds (Korol et al. 2020; Roebber et al. 2020; Keim et al. 2023) and possibly as far as the Andromeda galaxy (Korol et al. 2018). Here we outline the implications if such an opportunity arises. In Section 3.1 we illustrate the expected GW signal, assuming a double-degenerate scenario in which the primary white dwarf undergoes double detonation (Pakmor et al. 2022). While in Section 3.2 we briefly discuss the potential insights that could be gained from multi-messenger observations.

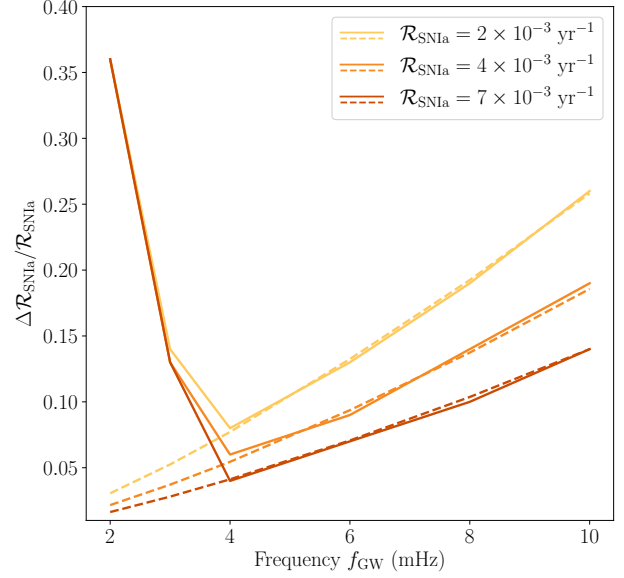


Fig. 3. LISA’s capability to measure SN Ia merger rate ($\mathcal{R}_{\text{SNIa}}$) from double-degenerate SN Ia progenitors at frequencies between 2 and 10 mHz for different values of the SN Ia rate. Solid lines represent the results of the Monte Carlo simulation where we combine uncertainties in the number count of SN Ia progenitors (assumed to be Poisson-distributed) with LISA’s ability to measure the chirp mass. Dashed lines show the number count error only.

3.1. Gravitational wave signal

To illustrate the GW signal from a WD+WD binary resulting in a SN Ia we adopt a 3D hydro-dynamical simulation of Pakmor et al. (2022). The simulation represents the last few orbits of a $1.05 M_{\odot}$ and $0.7 M_{\odot}$ carbon-oxygen WD+WD binary system, in which the primary undergoes the double-detonation mechanism (Livne 1990; Fink et al. 2010) via a dynamical ignition on the surface of the primary (Guillochon et al. 2010; Pakmor et al. 2013, 2022). To compute the GW signal based on the output of this simulation we perform the same calculations as Morán-Fraile et al. (2023). In Fig. 4 we show the evolution of GW frequency and strain as a function of time.

The first part of the signal (between -100 s to 0 s) represents the end of the inspiral phase starting with the onset of mass-transfer from the secondary ($0.7 M_{\odot}$) onto the primary ($1.05 M_{\odot}$) white dwarf via Roche-lobe overflow. During these 100 s the primary gains about $10^{-2} M_{\odot}$ of ${}^4\text{He}$. The evolution of the binary in this phase can be still be described as in Section 2, indeed the GW signal shows no significant deviation from a regular sinusoidal waveform.

At $t = 0$, the helium detonation ignites close to the point where the accretion stream hits the surface of the primary. The helium detonation then wraps around the primary burning its helium shell and sending a shockwave into its core. This shockwave converges in a single point in the core of the primary white dwarf and ignites a carbon detonation there at $t = 1.3 \text{ s}$. The carbon detonation completely burns and destroys the primary white dwarf ($t = 4.9 \text{ s}$) generating a SN Ia.

At the same time, the shockwave of the explosion of the primary hits the secondary white dwarf. It ignites the helium shell of the secondary at around $t = 2 \text{ s}$ and additionally sends a shock-

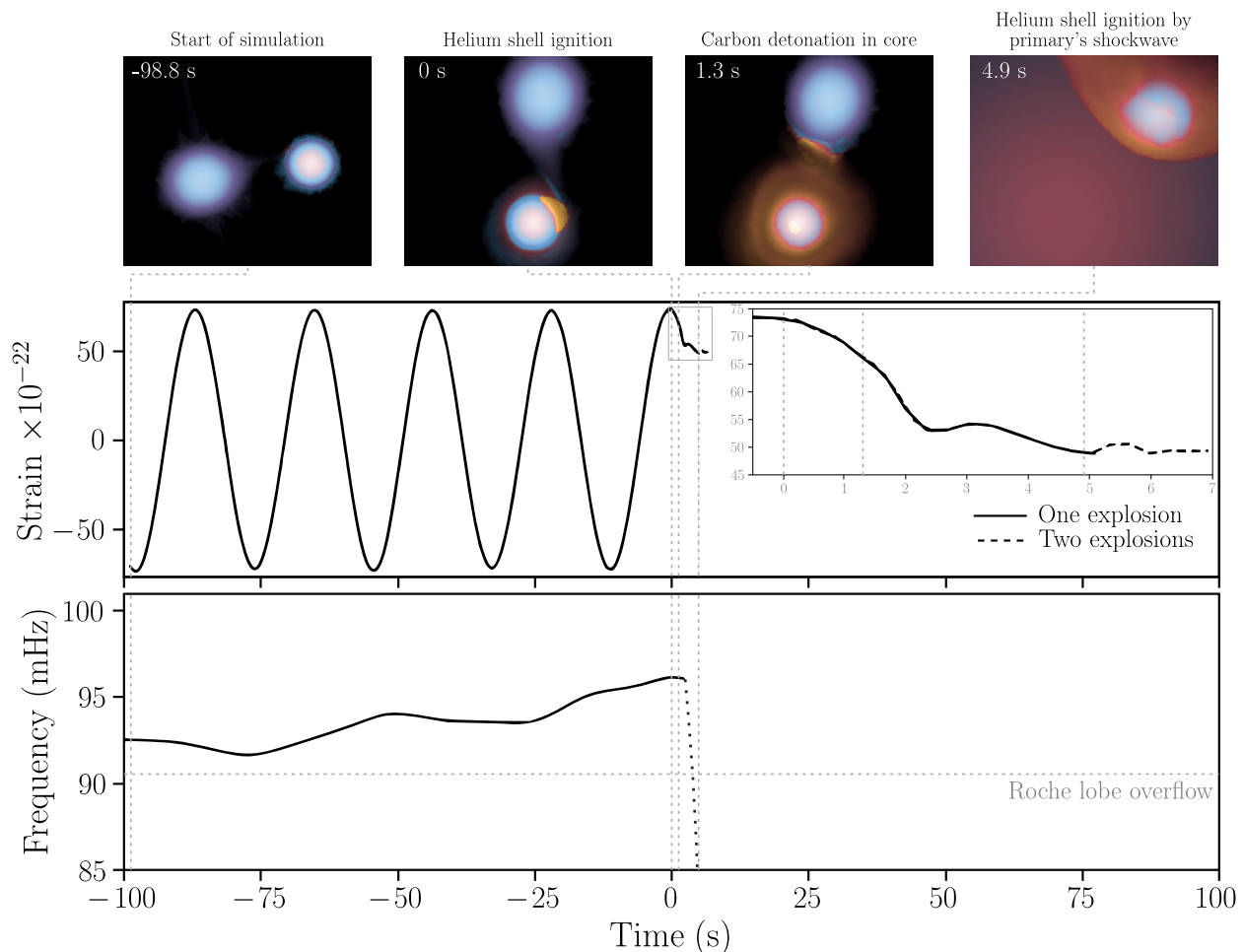


Fig. 4. GW frequency and strain as a function of time derived from the 3D hydro-dynamical simulation of $1.05 M_{\odot}$ and $0.7 M_{\odot}$ carbon-oxygen white dwarf binary of Pakmor et al. (2022). **Top panels:** Key steps of the double-detonation mechanism: $t = -98.8$ s, mass transfer from the secondary (visibly larger, fluffier white dwarf) onto the primary (more compact of the two); $t = 0$ s, helium-shell ignition on the primary; $t = 1.3$ s, the helium detonation wraps around the primary, triggering the detonation of the primary’s carbon-core; $t = 4.9$ s, the carbon detonation completely burns the primary (resulting in a SN Ia) and triggers helium-shell ignition on the secondary. **Middle panel:** The evolution of GW strain computed based on the output of the hydrodynamics simulation following the same method as in Morán-Fraile et al. (2023). The inset shows the zoom-in between -0.5 s and 7 s. The solid line shows ‘One explosion’ model, in which only the primary undergoes double detonation; the dashed line represents ‘Two explosions’ model, in which the explosion of the primary triggers double detonation of the secondary. **Bottom panel:** The solid line shows the evolution of GW frequency from the output of the simulation, transitioning into a dotted line when the primary is destroyed.

wave into its core directly. This shockwave, supported by the helium detonation burning the remaining helium around the secondary white dwarf converges in its core at $t = 4.9$ s. The converging shockwave in the secondary white dwarf fails to ignite a carbon detonation in its core and the secondary white dwarf survives until the end of the simulation 100 s later (‘One explosion’ model in Fig. 4). It is interesting to note that a detonation initiation in the secondary is physically plausible, given its density and temperature at $t = 4.9$ s. We show the GW signal for this possible scenario (‘Two explosions’) in the inset of Fig. 4 generated by artificially igniting a carbon detonation in the secondary at the convergence point of the shockwave. In this case, the second carbon detonation burns the secondary completely within about 1 s and destroys it as well.

Figure 4 illustrates that the binary emits nearly monochromatic GWs until just before the primary is disrupted by carbon detonation in the core, at which point the system virtually ceases to emit GWs. If the double detonation mechanism is responsible for a significant portion of normal SN Ia (resulting from a detonation of $0.8 - 1.1 M_{\odot}$ primary), the ignition and explosion must

occur prior to the merger, leading to a ‘clean’ disappearance of the binary’s GW signal as in our example (see also Seto 2023). If, on the other hand, the explosion occurs after the merger, such as in the case of the lower luminosity thermonuclear transient than a ‘normal’ SN Ia (e.g., resulting from the merger of a $0.6 M_{\odot}$ carbon-oxygen white dwarf with a $0.4 M_{\odot}$ helium white dwarf, see Morán-Fraile et al. 2024) the GW signal will comprise both the merger and post-merger phases until the double-detonation occurs. In this case, the delay between the merger and the explosion is of the order of several minutes. A more detailed description of this scenario will be provided in a dedicated study.

3.2. Chance of a multi-messenger observation

If a SN Ia occurs in the Milky Way while LISA is operational, we might observe a GW signal followed by the detection of EM signal (e.g., see synthetic light curves and spectra in Pakmor et al. 2022), followed by a shut off of the GW signal. Such an event would directly confirm the double-degenerate scenario, particularly demonstrating that SNe Ia are rapid dynamical ex-

plosions, unfolding over just a few seconds, as suggested by recent double-detonation models (cf. Section 3.1) or violent mergers (e.g., Pakmor et al. 2010, 2012). Any measurable delay between the GW and EM signals could indicate alternative detonation mechanisms and would represent an equally significant discovery.

A constraint on the progenitor binary component masses from the inspiral phase of the GW signal from LISA (cf. Section 2.2) and the observation of SN Ia would lead to a significant progress in modelling explosion physics of SNe Ia, even from a single observed event. Combining it with the EM signal would link the initial pre-explosion state of the system, and the outcome of the explosion in form of SN Ia ejecta and EM display. This would likely allow us to constrain and improve on the inherent uncertainties in the modelling of explosion physics for SNe Ia.

Observing a GW signal without a corresponding EM signal would also provide valuable insights, leading to several possible interpretations. First, with LISA's capability to localise WD+WD binaries within an area $\ll 1 \text{ deg}^2$ (e.g., Finch et al. 2023), it could allow us to confirm or exclude that no EM emission is detectable due to strong extinction. If extinction is ruled out, the absence of EM emission might suggest a traditional double-degenerate super-Chandrasekhar scenario (i.e., the merger of WD+WD with total mass exceeding Chandrasekhar mass limit) with a long delay that may extend up to 10^4 yr (e.g., Nomoto & Iben 1985; Shen et al. 2012). Finally, if an EM event is observed without a corresponding GW signal in the LISA band, this could indicate a single-degenerate scenario, where a GW signal in the LISA band is not expected, or a merger with a delay-time between merger and explosion longer than the observing time of LISA at this time.

In the fortunate event that we observe an SN Ia, this multi-messenger approach, leveraging both GW and EM information, promises a significant progress in our understanding of SN Ia, potentially directly resolving longstanding questions about their progenitors and provide crucial insights into the explosion mechanism.

4. Summary and conclusions

The nature of SN Ia have long been one of the most debated open questions in astrophysics. In this study, we review the expected insights that GW observations with LISA will provide about these transient phenomena. In particular, we argued that GW observations provide the most promising way for testing the so-called double-degenerate progenitor scenario, which involves a WD+WD binary that either interacts or merges via GW radiation resulting in a SN Ia. LISA's ability to survey WD+WD binaries across the entirety of the Milky Way makes it an ideal tool for testing this progenitor scenario.

In addition to LISA's science objective outlined in Colpi et al. (2024), we provided some additional quantitative estimates on the science that LISA will likely deliver in the context of SNe Ia:

- **A complete sample of Galactic WD+WD binaries with GW frequencies above 2 – 3 mHz**, corresponding to orbital periods shorter than 16 to 11 minutes. This implies that by simply counting WD+WD binaries in the LISA sample – without any concerns regarding selection effects – we will be able to estimate if there are enough double-degenerate binaries in the Milky Way to account for the observed SN Ia merger rate.

- **Constraints on the binary chirp mass to better than 1% at frequencies of 4–6 mHz**. This, in turn, will allow us to set a lower bound on the primary mass and to differentiate which WD+WD binaries in the LISA's sample will eventually result in a SN Ia ($m_1 > 0.8 M_\odot$).
- **Constraints on the merger rate of WD+WD binaries in the Milky Way to better than 4–9%**. If it turns out to be consistent with the SNe Ia rate measured based on EM observations in Milky Way-like galaxies, it would be persuasive evidence in favour of the double-degenerate scenario.

We also discussed the possibility of a direct observation of the final inspiral and SN Ia event, which, based on observational estimates, could have a likelihood of 3–7% for an extended LISA mission duration of 10 yr. We illustrated the expected GW signal for a double-degenerate scenario in which the primary white dwarf undergoes double detonation. In this case, the ignition and explosion of the primary occurs prior to the merger, leading to a 'clean' disappearance of the binary's quasi-monochromatic GW signal. We speculated that even a single multi-messenger detection would significantly advance the modelling of SN Ia explosions, reducing the parameter space on the initial conditions (based on constraints from the GW inspiral) and final EM ejecta. If we observe a quasi-monochromatic GW signal around 90 mHz – the exact frequency depends on the binary – followed by the detection of EM signal and a subsequent shut off of the GW signal, we would confirm the double-degenerate scenario in which SN Ia results from a double detonation of the primary white dwarf.

Acknowledgements. We thank Monica Colpi and Gijs Nelemans, who inspired this study while working on the LISA Definition Study Report (Red Book). Additionally, we thank Silvia Toonen, Alberto Vecchio, Alberto Sesana, Stephen Justham, and Carlos Badenes for their useful discussions and suggestions for this study.

References

- Amaro-Seoane, P., Andrews, J., Arca Sedda, M., et al. 2023, *Living Reviews in Relativity*, 26, 2
- Badenes, C. & Maoz, D. 2012, *ApJ*, 749, L11
- Breivik, K., Coughlin, S., Zevin, M., et al. 2020, *ApJ*, 898, 71
- Buscicchio, R., Klein, A., Roebber, E., et al. 2021, *Phys. Rev. D*, 104, 044065
- Buscicchio, R., Roebber, E., Goldstein, J. M., & Moore, C. J. 2019, *Phys. Rev. D*, 100, 084041
- Cappellaro, E. & Turatto, M. 2001, in *Astrophysics and Space Science Library*, Vol. 264, *The Influence of Binaries on Stellar Population Studies*, ed. D. Vanbeveren, 199
- Colpi, M., Danzmann, K., Hewitson, M., et al. 2024, arXiv e-prints, arXiv:2402.07571
- Fiacco, G., Cornish, N. J., & Yu, H. 2024, arXiv e-prints, arXiv:2405.10396
- Filippenko, A. V. 1997, *ARA&A*, 35, 309
- Finch, E., Bartolucci, G., Chucherko, D., et al. 2023, *MNRAS*, 522, 5358
- Fink, M., Röpke, F. K., Hillebrandt, W., et al. 2010, *A&A*, 514, A53
- GRAVITY Collaboration, Abuter, R., Amorim, A., et al. 2021, *A&A*, 647, A59
- Guillochon, J., Dan, M., Ramirez-Ruiz, E., & Rosswog, S. 2010, *ApJ*, 709, L64
- Hoyle, F. & Fowler, W. A. 1960, *ApJ*, 132, 565
- Huang, S.-J., Hu, Y.-M., Korol, V., et al. 2020, *Phys. Rev. D*, 102, 063021
- Iben, I., J. & Tutukov, A. V. 1984, *ApJS*, 54, 335
- Karnesis, N., Babak, S., Pieroni, M., Cornish, N., & Littenberg, T. 2021, *Phys. Rev. D*, 104, 043019
- Keim, M. A., Korol, V., & Rossi, E. M. 2023, *MNRAS*, 521, 1088
- Klein, A., Pratten, G., Buscicchio, R., et al. 2022, arXiv e-prints, arXiv:2204.03423
- Korol, V., Hallakoun, N., Toonen, S., & Karnesis, N. 2022, *MNRAS*, 511, 5936
- Korol, V., Koop, O., & Rossi, E. M. 2018, *ApJ*, 866, L20
- Korol, V., Rossi, E. M., Groot, P. J., et al. 2017, *MNRAS*, 470, 1894
- Korol, V., Toonen, S., Klein, A., et al. 2020, *A&A*, 638, A153
- Lamberts, A., Blunt, S., Littenberg, T. B., et al. 2019, *MNRAS*, 490, 5888
- Li, W., Chornock, R., Leaman, J., et al. 2011, *MNRAS*, 412, 1473

Table 1. Table with point estimates from simulations with BALROG, grouped sequentially by M_c , f , $\cos i$. Three leftmost columns are classification probabilities for each sources, according to the three classes: ‘No explosion’ ($m_1 < 0.5 M_\odot$), ‘Unde luminous’ ($0.5 M_\odot < m_1 < 0.8 M_\odot$) and ‘Normal SN Ia’ ($m_1 > 0.8 M_\odot$).

Injection parameters							Posterior				Classification %		
M_c^{inj} [M_\odot]	m_1^{inj} [M_\odot]	m_2^{inj} [M_\odot]	f^{inj} [Hz]	t_m^{inj} [Myr]	$\cos i^{\text{inj}}$	SNR	$\Delta M_c^{90\%}$ [M_\odot]	$\Delta t_m^{90\%}$ [Myr]	$\Delta M_c^{90\%} / M_c^{\text{inj}}$	$\Delta t_m^{90\%} / t_m^{\text{inj}}$	No expl. [%]	Underl. [%]	Normal [%]
0.42	0.60	0.40	0.002	1.345	0	5.1	5.57312	0.351	13.1211	0.2607	16.0	25.9	58.0
					1	15.0	0.64505	7.764	1.5187	5.7705	21.7	31.7	46.6
			0.006	0.072	0	57.4	0.00404	0.0011	0.0095	0.0159	3.4	56.0	40.6
					1	169.8	0.00137	0.0004	0.0032	0.0054	3.0	54.8	42.2
			0.010	0.018	0	82.0	0.00043	0.000031	0.0010	0.0017	3.1	55.3	41.6
					1	243.1	0.00015	0.00001	0.0003	0.0006	3.8	56.6	39.6
0.47	1.05	0.30	0.002	1.133	0	6.0	1.16005	5.589	2.4635	4.9332	18.1	25.6	56.3
					1	17.8	0.59892	6.316	1.2719	5.5747	19.3	33.2	47.4
			0.006	0.061	0	68.2	0.00313	0.0007	0.0067	0.0111	0.0	51.0	49.0
					1	201.7	0.00103	0.0002	0.0022	0.0037	0.0	51.2	48.8
			0.010	0.015	0	97.4	0.00033	0.000018	0.0007	0.0012	0.0	49.8	50.2
					1	288.7	0.00011	0.000006	0.0002	0.0004	0.0	51.5	48.5
0.74	1.05	0.70	0.002	0.529	0	12.9	0.71376	1.613	0.9603	3.0476	6.2	19.0	74.8
					1	38.1	0.23422	0.296	0.3151	0.5597	0.0	4.5	95.5
			0.006	0.028	0	146.0	0.00109	0.00007	0.0015	0.0024	0.0	0.0	100.0
					1	431.6	0.00037	0.00002	0.0005	0.0008	0.0	0.0	100.0
			0.010	0.007	0	208.5	0.00012	0.000002	0.0002	0.0003	0.0	0.0	100.0
					1	617.8	0.00004	0.000001	0.0001	0.0001	0.0	0.0	100.0

- Li, Z., Chen, X., Chen, H.-L., et al. 2020, ApJ, 893, 2
LISA Consortium Waveform Working Group, Afshordi, N., Akçay, S., et al. 2023, arXiv e-prints, arXiv:2311.01300
Liu, Z.-W., Röpke, F. K., & Han, Z. 2023, Research in Astronomy and Astrophysics, 23, 082001
Livio, M. & Mazzali, P. 2018, Phys. Rep., 736, 1
Livne, E. 1990, ApJ, 354, L53
Luo, J., Chen, L.-S., Duan, H.-Z., et al. 2016, Classical and Quantum Gravity, 33, 035010
Maoz, D., Badenes, C., & Bickerton, S. J. 2012, ApJ, 751, 143
Maoz, D., Hallakoun, N., & Badenes, C. 2018, MNRAS, 476, 2584
Maoz, D., Mannucci, F., & Nelemans, G. 2014, ARA&A, 52, 107
Moore, C. J., Cole, R. H., & Berry, C. P. L. 2015, Classical and Quantum Gravity, 32, 015014
Morán-Fraile, J., Holas, A., Röpke, F. K., Pakmor, R., & Schneider, F. R. N. 2024, A&A, 683, A44
Morán-Fraile, J., Schneider, F. R. N., Röpke, F. K., et al. 2023, A&A, 672, A9
Nelemans, G., Yungelson, L. R., Portegies Zwart, S. F., & Verbunt, F. 2001, A&A, 365, 491
Nomoto, K. & Iben, I. J. 1985, ApJ, 297, 531
Nomoto, K., Thielemann, F. K., & Yokoi, K. 1984, ApJ, 286, 644
Pakmor, R., Callan, F. P., Collins, C. E., et al. 2022, MNRAS, 517, 5260
Pakmor, R., Kromer, M., Röpke, F. K., et al. 2010, Nature, 463, 61
Pakmor, R., Kromer, M., Taubenberger, S., et al. 2012, ApJ, 747, L10
Pakmor, R., Kromer, M., Taubenberger, S., & Springel, V. 2013, ApJ, 770, L8
Perlmutter, S., Aldering, G., Goldhaber, G., et al. 1999, ApJ, 517, 565
Peters, P. C. 1964, Physical Review, 136, 1224
Portegies Zwart, S. F. & Verbunt, F. 1996, A&A, 309, 179
Rebassa-Mansergas, A., Toonen, S., Korol, V., & Torres, S. 2019, MNRAS, 482, 3656
Riess, A. G., Filippenko, A. V., Challis, P., et al. 1998, AJ, 116, 1009
Roebber, E., Busicchio, R., Vecchio, A., et al. 2020, ApJ, 894, L15
Ruan, W.-H., Guo, Z.-K., Cai, R.-G., & Zhang, Y.-Z. 2018, arXiv e-prints, arXiv:1807.09495
Ruiter, A. J. 2020, in White Dwarfs as Probes of Fundamental Physics: Tracers of Planetary, Stellar and Galactic Evolution, ed. M. A. Barstow, S. J. Kleinman, J. L. Provencal, & L. Ferrario, Vol. 357, 1–15
Sesana, A., Lamberts, A., & Petiteau, A. 2020, MNRAS, 494, L75
Seto, N. 2023, MNRAS, 523, 577
Shah, S. & Nelemans, G. 2014, ApJ, 791, 76
Shen, K. J. 2015, ApJ, 805, L6
Shen, K. J., Bildsten, L., Kasen, D., & Quataert, E. 2012, ApJ, 748, 35
Shen, K. J., Boos, S. J., & Townsley, D. M. 2024, arXiv e-prints, arXiv:2405.19417
Sim, S. A., Röpke, F. K., Hillebrandt, W., et al. 2010, ApJ, 714, L52
Tang, P., Eldridge, J., Meyer, R., et al. 2024, arXiv e-prints, arXiv:2405.20484
Thiele, S., Breivik, K., Sanderson, R. E., & Luger, R. 2023, ApJ, 945, 162
Toonen, S., Nelemans, G., & Portegies Zwart, S. 2012, A&A, 546, A70
Toubiana, A., Karnesis, N., Lamberts, A., & Miller, M. C. 2024, arXiv e-prints, arXiv:2403.16867
Whelan, J. & Iben, I. 1973, ApJ, 186, 1007
Wilhelm, M. J. C., Korol, V., Rossi, E. M., & D’Onghia, E. 2021, MNRAS, 500, 4958
Wolz, A., Yagi, K., Anderson, N., & Taylor, A. J. 2021, MNRAS, 500, L52